



ELSEVIER

Available online at [www.sciencedirect.com](http://www.sciencedirect.com)

SCIENCE @ DIRECT®

Nuclear Instruments and Methods in Physics Research A 527 (2004) 180–189

**NUCLEAR  
INSTRUMENTS  
& METHODS  
IN PHYSICS  
RESEARCH**  
Section A

[www.elsevier.com/locate/nima](http://www.elsevier.com/locate/nima)

## Monte Carlo simulation in PET and SPECT instrumentation using GATE

Karine Assié<sup>a</sup>, Vincent Breton<sup>b</sup>, Irène Buvat<sup>a</sup>, Claude Comtat<sup>c</sup>, Sébastien Jan<sup>c</sup>,  
Magalie Krieguer<sup>d</sup>, Delphine Lazaro<sup>b</sup>, Christian Morel<sup>e,\*</sup>, Martin Rey<sup>e</sup>,  
Giovanni Santin<sup>e,1</sup>, Luc Simon<sup>e,2</sup>, Steven Staelens<sup>f</sup>, Daniel Strul<sup>e,3</sup>,  
Jean-Marc Vieira<sup>e</sup>, Rik Van de Walle<sup>f</sup>

<sup>a</sup> U494 INSERM, CHU Pitié-Salpêtrière, Paris F-75634, Cedex 13, France

<sup>b</sup> Laboratoire de Physique Corpusculaire, Université de Clermont-Ferrand, Clermont-Ferrand F-63177, France

<sup>c</sup> Service Hospitalier Frédéric Joliot, CEA, Orsay F-91401, Cedex, France

<sup>d</sup> Inter-University Institute for High Energies, Vrije Universiteit Brussel, Brussels B-1050, Belgium

<sup>e</sup> Institute for High Energy Physics, University of Lausanne, Lausanne CH-1015, Switzerland

<sup>f</sup> ELIS Department, Ghent University, Ghent B-9000, Belgium

Members of the Crystal Clear Collaboration and of the OpenGATE Collaboration

---

### Abstract

Monte Carlo simulation is an essential tool to assist in the design of new medical imaging devices for emission tomography. On one hand, dedicated Monte Carlo codes have been developed for PET and SPECT. However, they suffer from a variety of drawbacks and limitations in terms of validation, accuracy, and/or support. On the other hand, accurate and versatile simulation codes such as GEANT3, EGS4, MCNP, and recently GEANT4 have been written for high energy physics. They all include well-validated physics models, geometry modeling tools and efficient visualization utilities. Nevertheless these packages are quite complex and necessitate a steep learning curve. GATE, the GEANT4 Application for Tomographic Emission, encapsulates the GEANT4 libraries in order to achieve a modular, versatile, scripted simulation toolkit adapted to the field of nuclear medicine. In particular, GATE allows the users to describe time-dependent phenomena such as detector movements or source decay kinetics, thus allowing to simulate time curves under realistic acquisition conditions. At present, it is being further developed and validated within the OpenGATE Collaboration. We give a succinct overview of GATE and four examples of its validation against real data obtained with PET and SPECT cameras.

© 2004 Elsevier B.V. All rights reserved.

PACS: 87.53.Wz; 87.58.Fg; 87.58.Ce

Keywords: Monte Carlo simulation; Nuclear medicine; Emission tomography; GATE; PET; SPECT

---

\*Corresponding author. Tel.: +41-21-693-0476; fax: +41-21-693-0477.

E-mail address: [christian.morel@iphe.unil.ch](mailto:christian.morel@iphe.unil.ch) (C. Morel).

<sup>1</sup> Present address: ESTEC, ESA, NL-2200 Noordwijk, The Netherlands.

<sup>2</sup> Present address: Institut Curie, Service de Physique Médicale, 26, rue d' Ulm, Paris F-75005, France.

<sup>3</sup> Present address: CNRS-LESIA, Observatoire de Meudon, F-92190 Meudon, France.

## 1. Introduction

Monte Carlo methods are extensively used in nuclear medicine to assist in the design of new medical imaging devices, new image reconstruction algorithms, or new scatter correction techniques for emission tomography. On one hand, dedicated Monte Carlo codes have been developed for Positron Emission Tomography (PET) and for Single Photon Emission Computerized Tomography (SPECT). However, these tools suffer from a variety of drawbacks and limitations in terms of validation, accuracy, and/or support [1]. On the other hand, accurate and versatile simulation codes such as GEANT3 [2], EGS4 [3], MCNP [4], and recently GEANT4 [5,6] have been written for high energy physics. They all include well-validated physics models, geometry modeling tools, and efficient visualization utilities. Nevertheless these packages are quite complex and necessitate a steep learning curve.

GATE, the GEANT4 Application for Tomographic Emission [7,8], encapsulates the GEANT4 libraries in order to achieve a modular, versatile, scripted simulation toolkit adapted to the field of nuclear medicine. In particular, GATE allows to describe time-dependent phenomena such as detector movements or source decay kinetics, thus allowing to simulate time curves under realistic acquisition conditions.

We present a succinct overview of GATE and four examples of its validation against real data obtained with PET and SPECT cameras.

## 2. GATE overview

GATE combines the advantages of the GEANT4 simulation toolkit—well-validated physics models, sophisticated geometry description, and powerful visualization and 3D rendering tools—with original features specific to emission tomography. It consists in several hundreds of C<sup>++</sup> classes. Mechanisms used to manage time, geometry, and radioactive sources form a core layer of C<sup>++</sup> classes close to the GEANT4 kernel. An application layer allows to implement user classes derived

from the core layer classes, e.g. to build specific geometrical volume shapes and/or to specify operations on these volumes like rotations or translations. Provided the application layer implements all appropriate features, the use of GATE does not require C<sup>++</sup> programming: a dedicated scripting mechanism that extends the native command interpreter of GEANT4 [6] allows to perform and to control Monte Carlo simulations of realistic setups. Fig. 1 illustrates the construction of a PET scanner comprising 10 sectors of four modules of 8 × 8 LSO crystals (1 × 1 × 8) mm<sup>3</sup> by using the following set of scripting lines:

```
# Define class hierarchy world ← scanner ←
sector ← module ← crystal
/gate/world/daughter/name scanner
/gate/scanner/daughter/name sector
/gate/sector/daughter/name module
/gate/module/daughter/name crystal

# Define crystal geometry
/gate/crystal/geometry/setXLength 10 mm
/gate/crystal/geometry/setYLength 1 mm
/gate/crystal/geometry/setZLength 1 mm

# Define crystal material
/gate/crystal/setMaterial LSO

# Repeat crystal in a cubic array
/gate/crystal/repeaters/insert cubicArray
/gate/crystal/cubicArray/setRepeatNumberX 1
/gate/crystal/cubicArray/setRepeatNumberY 8
/gate/crystal/cubicArray/setRepeatNumberZ 8
/gate/crystal/cubicArray/setRepeatVector 0.
2.25 2.25 mm

# Repeat module in a cubic array
/gate/module/repeaters/insert cubicArray
/gate/module/cubicArray/setRepeatNumberZ 2
/gate/module/cubicArray/setRepeatNumberY 2
/gate/module/cubicArray/setRepeatVector 0
19.75 19.75 mm

# Repeat sector in a ring
/gate/sector/repeaters/insert ring
/gate/sector/ring/setRepeatNumber 10
```

One of the most innovative features of GATE is its capability to synchronize all time-dependent components in order to allow a coherent description of the acquisition process. The elements of the geometry can be set into movement via scripting again. For example, the scanner described above can be set into

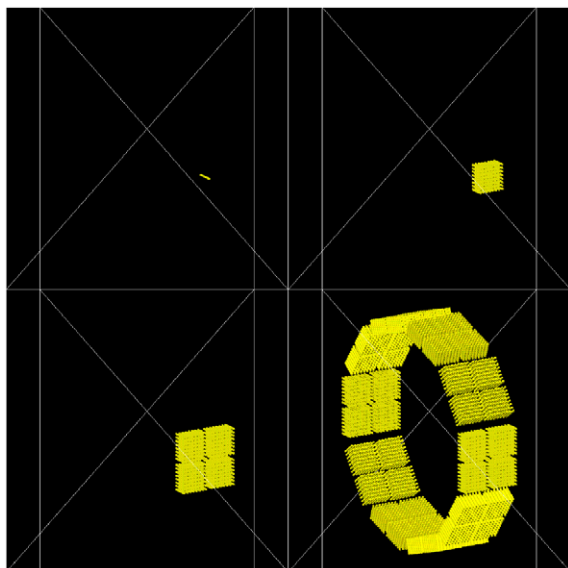


Fig. 1. Example of the construction of a device comprising 10 sectors of four modules of  $8 \times 8$  crystals. Top left: definition of the crystal geometry. Top right: definition of the module geometry by repeating the crystal geometry in a  $8 \times 8$  array. Bottom right: definition of the sector geometry by repeating the module geometry in a  $4 \times 4$  array. Bottom left: definition of the scanner geometry by repeating the sector geometry 10 times around a ring.

rotation simply by using the following scripting lines:

```
# Define scanner movement
/gate/scanner/moves/insert rotation
# Set rotation speed
/gate/scanner/rotation/setSpeed 3.6 deg/s
```

All movements of the geometrical elements are kept synchronized with the evolution of the source activities. For this purpose, the acquisition is subdivided into a number of time-steps during which the elements of the geometry are considered to be at rest. Decay times are generated within these time-steps so that the number of events decreases exponentially from time-step to time-step, and decreases also inside each time-step according to the decay kinetics of each radioisotope. This allows to model time-dependent processes such as count rates or detector dead-time on an event-by-event basis [9]. Moreover, the GEANT4 interaction histories are used to mimic realistic detector output. Detector electronic response is modeled as a chain of

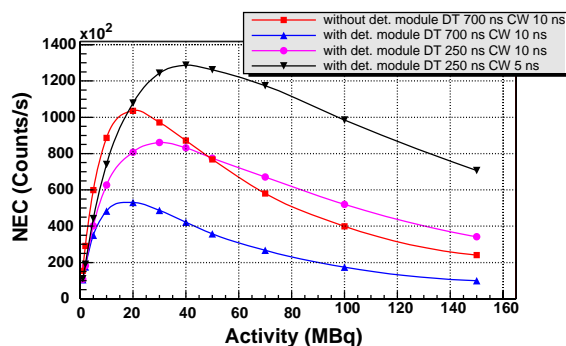


Fig. 2. NEC curves determined for different combinations of detector dead-times (DT = 700 or 250 ns) and coincidence time windows (CW = 10 or 5 ns). Squares are obtained without modeling the detector electronic response. All other points are obtained with a model of the detector electronic response including detector cross-talk, transfer efficiency of the scintillation photons to the photo-detector, quantum efficiency of the photo-detector, detector energy resolution, and trigger efficiency.

processing modules designed by the user to reproduce e.g. the detector cross-talk, its energy resolution, or its trigger efficiency. Fig. 2 shows several Noise Equivalent Count (NEC) curves determined for a small animal PET scanner design using various detector dead-times and/or coincidence time windows. Depending on the model used for the detector electronic response and for the time-dependent processes, the NEC curves shown in Fig. 2 are significantly different. This demonstrates the uppermost importance of modeling accurately both the detector and the time-dependent processes in order to derive meaningful information from Monte Carlo simulations of emission tomographs.

### 3. Validation of gate

Validation of Monte Carlo results against real data obtained with PET and SPECT cameras is essential to assess the accuracy of the simulations. In this section, we present four specific examples of the validation of GATE against existing medical imaging devices.

#### 3.1. ECAT EXACT HR+

The PET camera ECAT EXACT HR+ (CPS Innovations) [10] uses BGO blocks cut into  $8 \times 8$

arrays of crystals ( $4.0 \times 4.1 \times 30$ ) mm<sup>3</sup> each. In this camera, 2304 detectors are arranged in 32 axial rings to form a 82.7 cm diameter detector cylinder. The axial length of the Field-Of-View (FOV) is 15.5 cm. The simulation of the HR+ camera assumed a global energy resolution of 25% at 511 keV. As for the experimental data, a 350–650 keV energy window, and a 12 ns coincidence time window were applied. Three sets of simulations are presented and compared to experimental data: scatter fraction estimates, spatial resolution measurements, and absolute sensitivity measurements. For the HR+ sensitivity and for the scatter fraction estimates, the NEMA NU-2 1994 protocol [11] was applied to both the simulated and the experimental data. Both for the simulation and for the experimental measurements, we used a 1.0 mm diameter, 1.0 mm height cylindrical <sup>18</sup>F aqueous source embedded in a 5 cm long capillary tube with 2 mm external diameter to estimate image resolution. The source was placed at five radial offset locations of 1, 5, 10, 15, and 20 cm. Two decay modes were simulated: explicit emission of the positrons by taking into account their range and the acolinearity of the annihilation photons (hereafter referred to as the <sup>18</sup>F decay mode), and direct back-to-back emission of two 511 keV gammas at the decay location (hereafter referred to as the  $\gamma/\gamma$  mode). Simulated and experimental data were reconstructed with the non-apodized 3D Re-Projection (3DRP) algorithm [12], with a zoom factor of 10.

### 3.1.1. Results

In the 3D acquisition mode, the mean simulated value of the total scatter fraction was about 35%. This result is in good agreement with the experimental calculation, which amounts to 36%. Fig. 3 shows the differences between GATE simulated and experimental data for the radial resolutions (i.e. FWHM and FWTM values of the radial profiles). Simulation results are always lower than experimental measurements. The mean value of the discrepancy is about 7% with the <sup>18</sup>F decay mode, and 11% with the  $\gamma/\gamma$  mode. These results reflect the fact that only energy depositions within the crystals were simulated explicitly. Neither the scintillation, nor the light collection processes were

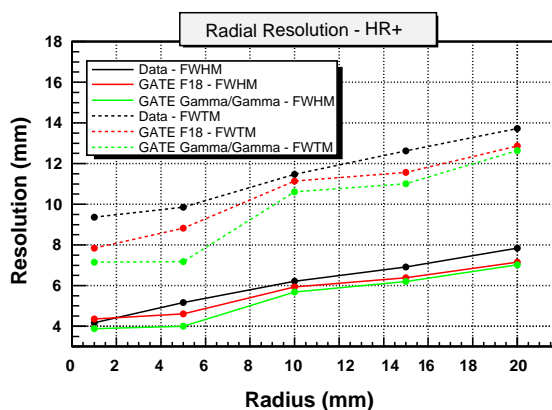


Fig. 3. Evaluation of the spatial resolution (FWHM and FWTM) with GATE ( $\gamma/\gamma$  mode and <sup>18</sup>F decay mode) compared with experimental values.

modeled. These effects can be accounted for with an appropriate analytic blurring function applied to the detection position of the photon within the crystal.

The absolute sensitivity and scatter fraction estimates were performed using a standard 20 cm diameter, 20 cm height water cylinder phantom filled with aqueous <sup>18</sup>F. After scatter fraction correction, the simulation by GATE gave an absolute sensitivity of 0.8%. This result is in very good agreement with the experimental measurement, which amounts to 0.75%.

### 3.2. Dual-headed SPECT

GATE simulations were validated through comparison with experimental data measured on a dual-headed AXIS camera (Philips), which was extensively modeled to represent the physical reality (Fig. 4). In order to achieve accurate descriptions of Low Energy High Resolution (LEHR) and Medium Energy General Purpose (MEGP) collimators, the air holes had to be modeled according to the technical specifications of these collimators, particularly their hole diameter and their septal thickness. For this purpose, a typical hexagonal shape was added to the GATE geometry package.

The construction of the lead collimators was performed by repeating a hexagon on a rectangular array. This array was then filled up with a

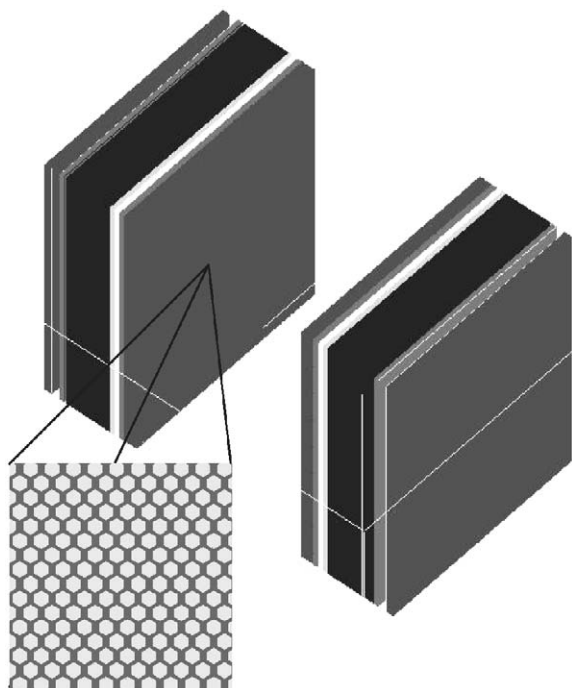


Fig. 4. View of the modeled AXIS detector heads with a zoom on the collimator.

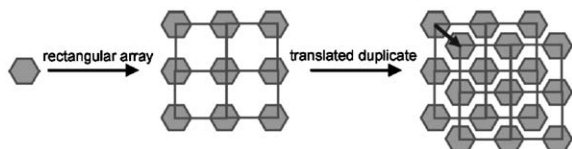


Fig. 5. Detail of the collimator modeling process.

translated duplicate, hence creating the complete distribution of air holes, as shown in Fig. 5.

Examples of validated properties include the spectral distributions, sensitivity and spatial resolution.

### 3.2.1. Spectral distributions

The scintillation process and the light detection were not incorporated in our model. An “energy blurrer” was used instead that introduced a Gaussian energy distribution with user-defined mean and standard deviation. We adapted the energy module to obtain an energy-dependent spectral resolution following  $1/\sqrt{E}$  with an overall

resolution of 9.5% at 140.5 keV, which corresponds to the energy resolution quoted by the manufacturer for the real detector. The spectral distributions were validated by the following study: real data were taken with a 29 MBq  $^{99m}\text{Tc}$  point source placed at 15 cm from the collimator surface, and the results were compared to the energy spectrum simulated with GATE in an identical configuration. In a second phase, the same source was inserted in a cylindrical water-filled phantom, placed at 10 cm from the detector surface. The resulting spectra were plotted together with the simulation results (Fig. 6).

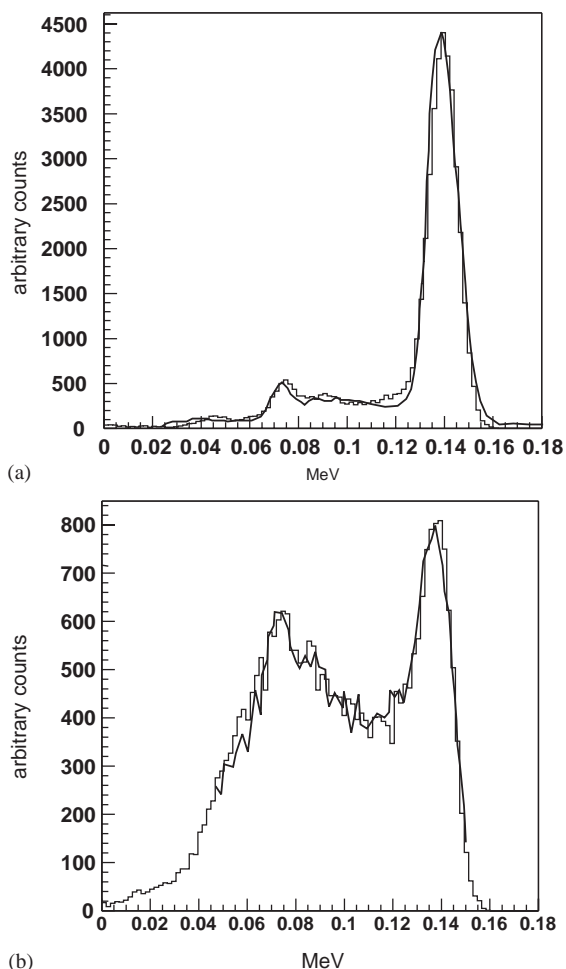


Fig. 6. Comparison of simulated and measured  $^{99m}\text{Tc}$  spectra: (a) source in air; (b) source in water scattering medium. Line: measurement; histogram: simulation.

### 3.2.2. Sensitivity

We evaluated the sensitivity in two separate windows to make sure that there were no additive effects in the simulations. In a first experiment, we performed a static scan with the LEHR collimator of a point source—a 1 ml sphere filled with 2.6 MBq  $^{99m}\text{Tc}$ —placed at 5, 15, 25, and 30 cm from the detector surface. We acquired data in the photopeak window (129–151 keV), and in the Compton window (92–126 keV). We set up corresponding simulations for each experiment and then compared the simulated and experimental sensitivities. Error bars were added due to the imprecision on the activity of the  $^{99m}\text{Tc}$  source. In Fig. 7, the results are shown for the photopeak, and for the Compton window. We see a good agreement within the range of the error bars between the experiments and the simulations.

### 3.2.3. Spatial resolution

A “spatial blurrer” module was created to model the intrinsic spatial resolution caused by crystal scatter and by the electronic readout. The extrinsic resolution caused by all other parts of the detector was also simulated. In order to check the validity of the spatial blurrer for the intrinsic resolution and of the collimator model, a series of experiments was conducted.

We performed scans of a line source phantom of 0.1 cm diameter and 5 cm height, filled with 19 MBq  $^{99m}\text{Tc}$ , and placed at 5, 10, 20, and 40 cm from the detector mounted with the LEHR

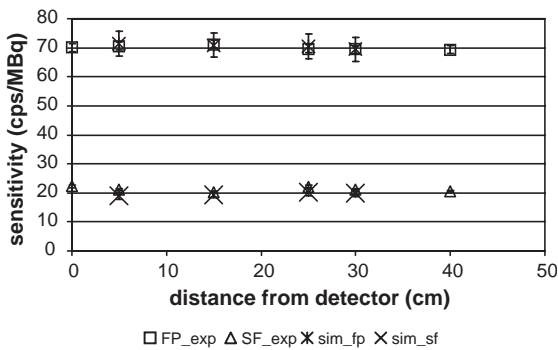


Fig. 7. Sensitivity validation for the LEHR collimator: FP: photopeak window (129–51 keV); SF: Compton window (92–126 keV).

collimators. The FWHM of each acquisition was determined. The same procedure was used for the simulations. It was repeated for a line source of 0.2 cm diameter filled with 66 MBq  $^{99m}\text{Tc}$  placed at 5, 15, 26.9, 35, and 45 cm from the detector surface with the MEGP collimators attached to it. Fig. 8 shows the result of the spatial resolution experiments where the simulated FWHMs are compared with the measured FWHMs of line sources in air. Good agreement is reached within the error bars both for the LEHR and for the MEGP collimator.

### 3.3. $^{111}\text{In}$ SPECT

Accurate quantification of SPECT images would be extremely useful for dosimetric calculation in radio-immunotherapy, when the in vivo distribution of the therapeutic agent, e.g. ZEVALIN<sup>®</sup> labeled with  $^{90}\text{Y}$  for the treatment of non-Hodgkin lymphoma, can be a priori determined using a SPECT scan of a radiotracer presenting the same bio-distribution as the therapeutic agent, such as ZEVALIN<sup>®</sup> labeled with  $^{111}\text{In}$ . Monte Carlo simulations are an appropriate tool to assess the quantitative accuracy achievable from  $^{111}\text{In}$  SPECT images as a function of the correction and reconstruction schemes. However, validation of

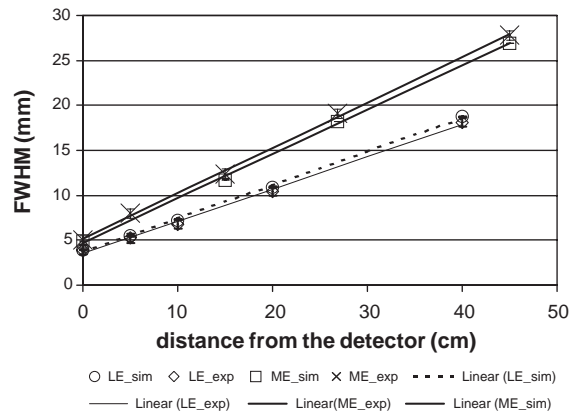


Fig. 8. Comparison of spatial resolution for an LEHR and for an MEGP collimator: LE\_sim shows the simulated spatial resolutions, and LE\_exp shows the acquired spatial resolutions for the LEHR collimator. ME\_sim and ME\_exp illustrate simulated and acquired spatial resolutions for the MEGP collimator; a linear curve is fitted to each data plot.

Monte Carlo simulation codes for  $^{111}\text{In}$  SPECT has not been reported so far. We were thus interested in validating GATE for  $^{111}\text{In}$  SPECT imaging.

In that context, GATE allowed us to model the two emission energies of  $^{111}\text{In}$  (171 and 245 keV), and the DST-Xli (General Electric) imaging device. The photon interactions were modeled in a precisely defined Medium Energy High Resolution collimator, in the 3/8" thick NaI crystal, in a back-compartment, in the head shielding, and in the table. The spatial resolution loss due to the photomultiplier tubes and to the associated electronics was modeled by convolution of the simulated data with a 1.6 mm FWHM Gaussian, as determined by comparing the known intrinsic camera spatial resolution with the spatial resolution loss due to the crystal only estimated by the simulation. Energy resolution measurements on the camera enabled us to set the energy resolution to 10% at 171 keV and at 245 keV.

### 3.3.1. Results

The simulation accuracy was tested by comparing measured and simulated energy spectra from 49 to 281 keV for a line source in air located at 10 cm from the collimator surface, and for a line source 5 cm deep in a  $(30 \times 30 \times 30)$  cm<sup>3</sup> water tank located at 8 cm from the collimator surface (Fig. 9). It was also assessed by comparing the spatial resolution characterized by the FWHM estimate for line sources in air located at different distances from the collimator surface (Table 1), and by comparing sensitivity values obtained for the line sources in air experiments (Table 2).

As illustrated by the examples shown above, a comprehensive analysis of our validation results concerning spatial resolution, sensitivity, energy spectra, scatter fractions, and image recovery suggests that GATE allows accurate simulation of  $^{111}\text{In}$  SPECT imaging, especially due to its ability to accurately simulate interactions within the collimator equipping the camera. GATE therefore appears to be an appropriate tool to characterize the quantitative accuracy of an acquisition, and of the processing protocols used in  $^{111}\text{In}$  SPECT.

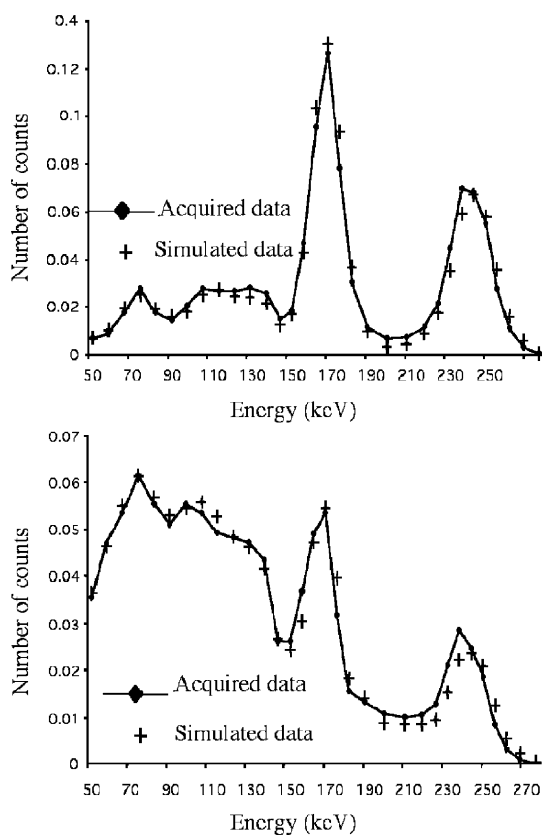


Fig. 9. Simulated and acquired  $^{111}\text{In}$  energy spectra for a line source in air (left) and in water (right).

Table 1  
FWHM in mm for different  $^{111}\text{In}$  line source-to-collimator distances obtained from simulations and real experiments in air

Source-to-collimator distance (mm)	0	50	100	150	200
Simulations	5.7	7.0	9.6	11.5	14.4
Measurements	5.8	7.0	9.5	11.5	14.2

### 3.4. Small animal gamma camera

A small animal gamma camera prototype tested at IASA (Institute of Accelerating Systems and Applications of Athens) [13] was modeled using GATE. It is made of a 3 mm-thick CsI(Tl) crystal array of  $41 \times 41$  orthogonally arranged pillars

Table 2

Sensitivity values ( $\times 10^{-4}$ ) for different  $^{111}\text{In}$  line source-to-collimator distances obtained from simulations and real experiments in air

Source-to-collimator distance (mm)	0	50	100	150	200
Simulations	1.9	1.7	1.7	1.7	1.7
Measurements	1.8	1.8	1.8	1.8	1.8

coupled to a position sensitive photomultiplier tube (PS-PMT) R2486 manufactured by Hamamatsu. The gamma camera head is equipped with an LEHR parallel-hole collimator. Direct access to the anode wire signals is provided, hence allowing to compute the photon interaction position and its energy, and to compare them to simulated values.

The whole detection chain was modeled, including the physical interactions in the LEHR collimator, in the crystal pixels, and in the PS-PMT. The backscatter on the PS-PMT glass entrance window is a major component of the energy spectrum as the crystal is only 3 mm thick, and it must be taken into account. The intrinsic performances of the prototype, as well as the intrinsic spatial and energy resolutions were determined by measurements, and used in the simulations to reproduce the intrinsic detection response of the gamma camera.

### 3.4.1. Results

The basic performances of the gamma camera—Point Spread Functions (PSFs), and energy spectra—in planar scintigraphic imaging were measured on the prototype in several configurations, and then compared to the results given by the simulations. The PSFs were experimentally measured with a  $^{99\text{m}}\text{Tc}$  point source centered in the FOV. The source was a 1.3 diameter capillary of 2 mm length filled with 0.49 MBq activity, and located in air at 2, 5, and 10 cm from the collimator surface. Images were obtained for a 40–180 keV energy window. A profile through the point source was drawn for each of the three images, and the FWHM values were calculated. The energy spectra were experimentally measured on the whole FOV: (1) in air with the 0.49 MBq

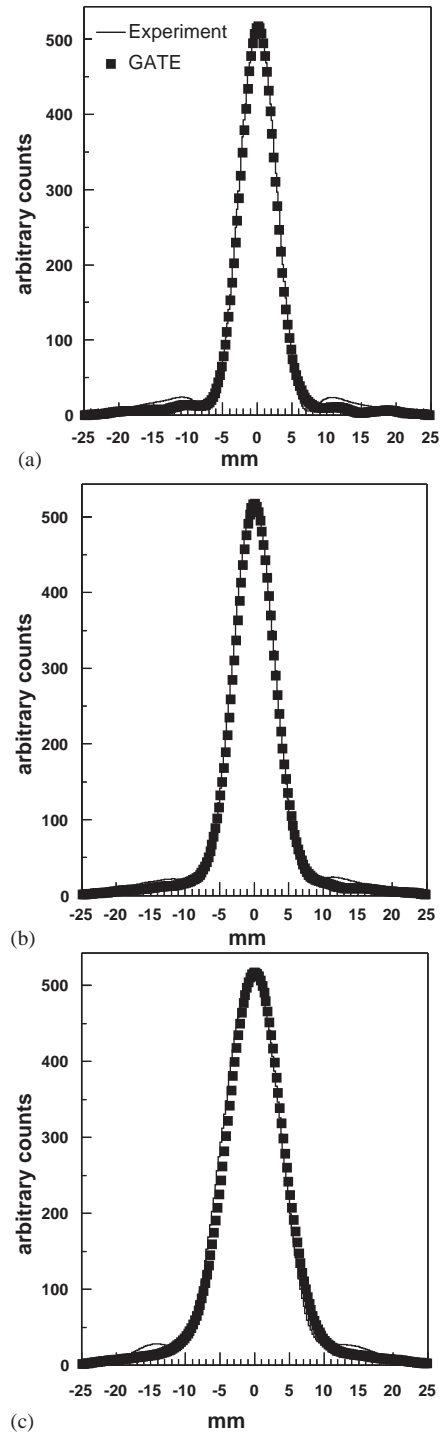


Fig. 10. Measured and GATE simulated point spread functions for a centered  $^{99\text{m}}\text{Tc}$  point source located at: (a) 2 cm, (b) 5 cm, and (c) 10 cm from the camera.

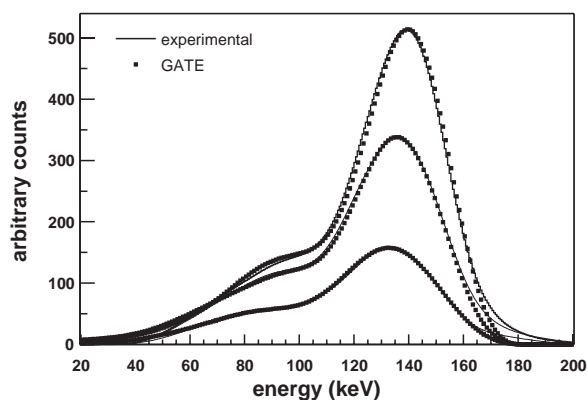


Fig. 11. Energy spectra obtained for the  $^{99\text{m}}\text{Tc}$  point source at 12 cm from the collimator under a water thickness of 4 cm (middle curve) and of 10 cm (top curve). The energy spectrum obtained for 0 cm of water is shown as reference (bottom curve).

$^{99\text{m}}\text{Tc}$  point source located at 2 cm from the collimator surface, (2) in water with a 5.11 MBq  $^{99\text{m}}\text{Tc}$  point source located at 12 cm from the collimator surface, below a cylindrical phantom filled with 4 cm, or with 10 cm water. Five million photon histories were simulated in the acceptance angle of the gamma camera. The simulated PSFs determined for the three source-to-collimator distances were compared to the experimental measurements (Fig. 10). The comparison of the three energy spectra simulated in air, and in water are shown in Fig. 11.

A very good agreement is found for the simulation of the FWHM, with differences of less than  $100\ \mu\text{m}$  between the simulated and the experimental values. Small discrepancies can be noticed in the tails of the PSFs, which can be attributed to an experimental problem of charge collection on the PS-PMT wires.

The comparison between the experimental and the simulated energy spectra demonstrates the very good agreement that was achieved with GATE. Some differences may be seen between 80 and 100 keV, because the X-rays created in the collimator were probably being slightly overestimated in the simulation. At the high energy end of the spectrum, the experimental data show a tail of pulses between 170 and 200 keV, which was not accounted for by the Gaussian blurring model.

#### 4. Conclusion and future prospects

Further validation and development of GATE is carried on within the OpenGATE Collaboration [14] with the objective to provide the academic community with a free, general-purpose, GEANT4-based simulation platform for emission tomography. The Collaboration comprises more than 20 laboratories fully dedicated to the task of improving, documenting, and testing GATE thoroughly against most of the imaging systems commercially available in PET and SPECT [15,16]. This will hopefully ensure the long term support and continuity of GATE, which we intend to set up as a new standard for Monte Carlo simulation in nuclear medicine.

#### Acknowledgements

This work was supported by the Swiss National Science Foundation under Grants No. 2153-063870 and No. 205320-100472, and by the Institute for the Promotion of Innovation by Science and Technology in Flanders (IWT, Belgium).

#### References

- [1] I. Buvat, I. Castiglioni, *J. Nucl. Med.* 46 (2002) 48.
- [2] R. Brun, F. Bruyant, M. Maire, A.C. McPherson, P. Zanarini, "GEANT3," CERN DD/EE/84-1, 1987.
- [3] Electron Gamma Shower (EGS) transport code: <http://www.slac.stanford.edu/egs/>.
- [4] Monte Carlo N-Particle (MCNP) transport code: <http://laws.lanl.gov/x5/MCNP/index.html>.
- [5] Geometry And Tracking (Geant) transport code: <http://www.cern.ch/geant4>.
- [6] S. Agostinelli, et al., *Nucl. Instr. and Meth. A* 506 (2003) 250.
- [7] D. Strul, G. Santin, D. Lazaro, V. Breton, C. Morel, GATE (Geant4 Application for Tomographic Emission): a PET/SPECT general-purpose simulation platform, *Nucl. Phys. B (Proc. Suppl.)* 125 (2003) 75–79.
- [8] G. Santin, D. Strul, D. Lazaro, L. Simon, M. Krieguer, M. Vieira Martins, V. Breton, C. Morel, GATE, a Geant4-based simulation platform for PET and SPECT integrating movement and time management, *IEEE Trans. Nucl. Sci.* 50 (2003) 1516–1521.

- [9] L. Simon, D. Strul, G. Santin, M. Krieguer, C. Morel, Simulation of time curves in small animal PET using GATE, Nucl. Instr. Meth. A, [these Proceedings](#).
- [10] G. Brix, J. Zaers, L.E. Adam, M.E. Bellemann, H. Ostertag, H. Trojan, U. Haberkorn, J. Doll, F. Oberdorfer, W.J. Lorenz, J. Nucl. Med. 38 (1997) 1614.
- [11] National Electrical Manufacturers Association, NEMA Standards Publication NU 2-1994, Performance measurements of positron emission tomographs, Washington, DC, 1994.
- [12] P.E. Kinahan, J.G. Rogers, IEEE Trans. Nucl. Sci. NS-36 (1989) 964.
- [13] G.K. Loudos, K.S. Nikita, N.D. Giokaris, E. Styliaris, S.C. Archimandritis, D. Varvarigou, et al., A 3D high-resolution gamma camera for radiopharmaceutical studies with small animals, Appl. Radiat. Isot. 58 (2003) 501–508.
- [14] OpenGATE Collaboration: <http://www-lphe.epfl.ch/GATE>.
- [15] S. Staelens, D. Strul, G. Santin, M. Koole, S. Vandenberghe, Y. D'Asseler, I. Lemahieu, R. Van de Walle, Monte Carlo simulations of a scintillation camera using GATE: validation and application modeling, Phys. Med. Biol. 48 (2003) 3021–3042.
- [16] D. Lazaro, I. Buvat, G. Loudos, D. Strul, G. Santin, N. Giokaris, D. Donnarieix, L. Maigne, V. Spanoudaki, S. Styliaris, S. Staelens, V. Breton, Validation of the GATE Monte Carlo simulation platform for modelling a CsI(Tl) scintillation camera dedicated to small-animal imaging, Phys. Med. Biol. 49 (2003) 271–285.